Physical self-assembly and the nucleation of three-dimensional nanostructures by oblique angle deposition

T. Karabacak,[a] G.-C. Wang, and T.-M. Lu
Department of Physics, Applied Physics and Astronomy, Rensselaer Polytechnic Institute, Troy, New York 12180-3590

(Received 24 October 2003; accepted 22 March 2004; published 22 July 2004)

Growth front morphology of a thin film formed by physical vapor deposition is controlled by many factors including surface diffusion and shadowing effects. Instabilities can occur if shadowing is more dominant compared to other surface effects and can lead to many diverse physically self-assembled three-dimensional nano-size structures. In this article, we explore the fundamental nucleation and growth mechanisms of the nanostructures during oblique angle deposition. Monte Carlo simulations were carried out to predict the island density, island size distribution, and island–island correlation during the initial stages of growth. The results were compared to that obtained by the oblique angle sputter deposited tungsten films imaged by atomic force microscopy and scanning electron microscopy. Isolated islands with quasiperiodic distribution were formed as a natural consequence of the shadowing effect. Isolated columnar structures are shown to grow on these islands and the width W of the columns is predicted to grow as a function of column length d in a power law form, $W \sim d^p$, where the exponent p is between 0.3 and 0.5. The predicted p is consistent with the experimentally determined exponent values for growth of column widths from a variety of materials such as W, Co, Cu, and Si. The exponent values calculated from a derived continuum equation were also consistent with the experimental results. © *2004 American Vacuum Society.*
[DOI: 10.1116/1.1743178]

I. INTRODUCTION

Oblique angle deposition technique[1–6] (also known as glancing angle deposition) can generate nanostructures relatively easily and has attracted the interest of many researchers. In oblique angle growth, one modifies the substrate holder of a typical deposition system to be able to rotate and tilt. Due to the shadowing effect, the incident particles of a material that come to the surface with an oblique angle are preferentially deposited on the top of surface features with larger values in height. This preferential growth dynamic gives rise to the formation of isolated nanostructures. Figure 1(a) shows an example of silicon columnar structure obtained at a large oblique angle $\theta = 85°$ (measured from the surface normal) with substrate rotation and imaged by scanning electron microscopy (SEM). Many nanostructures of technological interest (besides columns) can be obtained by simply controlling the deposition angle, deposition rate, rotation speed, and material specific parameters such as surface diffusion and crystal plane effects. Figures 1(b)–1(d) show some other three-dimensional (3D) geometry such as nanosprings and nanoballs, which were recently fabricated in our labs.

In 1959, Young and Kowal[1] realized the fabrication of the first thin film helicoidal bianisotropic mediums. Using a physical vapor deposition technique, they deposited a tilted columnar thin film, while simultaneously rotating the substrate about an axis normal to the substrate. In 1989, thin film retardation plates of various ceramics were produced by Motohiro and Taga in oblique incidence electron-beam evaporation experiments.[2] In this work, the birefringence properties of obliquely deposited, tilted columnar and zigzag shaped films were investigated, and favorable conditions for the formation of high retardation, low opacity quarterwave plates were identified. Shortly after, Azzam proposed a method of producing chiral thin solid films to be used in quadrant-detector ellipsometers.[3] The viability of the oblique angle deposition technique was first demonstrated by Robbie *et al.*,[4] who used SEM to show a variety of many interesting nanostructures. The nanostructures created with oblique angle deposition were studied for their optical,[1–3,7–11] mechanical,[12–14] magnetic,[15–17] structural,[18,19] and electrical[20] properties. Nanostructures made for photonic crystals,[21,22] field emitters,[23,24] thermal transport/barrier layers,[25,26] and thermal layers in microchannels[27,28] have also been investigated. The fabrication of periodic structures was achieved by using regularly spaced seed elements of colloids[29] or pillars[30,31] as starting template surfaces.

Although the oblique angle deposition with substrate rotation can fabricate very attractive structures full of interesting physical properties, there has been little detailed work reported on the study of the growth dynamics. Moreover, the published theoretical studies were mostly for the cases of no substrate rotation, which basically produced slanted columns.[32–41] Vick, Smy, and Brett[42] created (2+1) Monte Carlo (MC) simulations that included both substrate rotation and surface diffusion effects, and has been used to calculate the root mean square roughness of columnar interface. In addition, Smy *et al.*, using a (2+1) MC simulator, which included surface diffusion and substrate rotation effects, suc-

[a]Author to whom correspondence should be addressed; electronic mail: karabt@rpi.edu

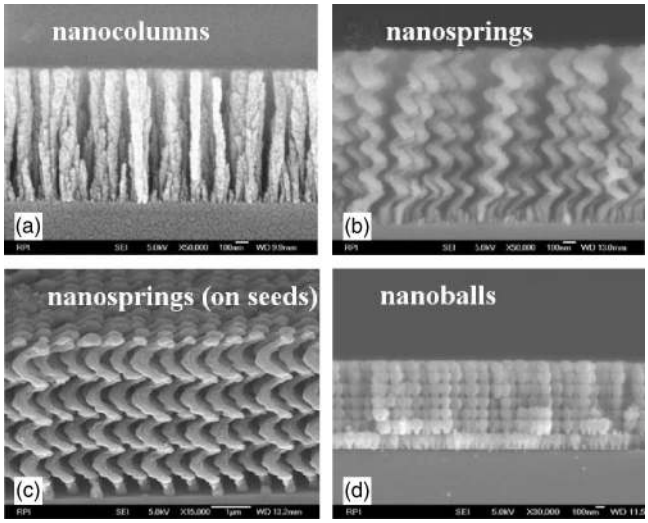

FIG. 1. SEM cross-section images of some nanostructures obtained by oblique angle deposition. All nanostructures are made of silicon.

cessively obtained nanostructures of spring, column, and zigzag shapes that are qualitatively similar to experimental results.[43] Suzuki and Taga also used a (2+1) MC simulation method to predict the effective surface area of nanostructures with various shapes.[44]

This article aims to analyze quantitatively the growth dynamics of oblique angle deposition in much more detail, and present an overall understanding of the growth process. The growth regimes studied cover the deposition times from very early stages of island growth to later stages of columnar structures. One may expect that, at initial times, the islands are mostly two-dimensional (2D) and the nucleation mechanisms are quite different compared to that of normal angle deposition.[45–47] The shadowing effects can introduce interesting results, in particular, about the island size distribution, island density, and island–island correlation. As the deposition proceeds, we expect a transition from 2D island structures to three-dimensional (3D) columnar structures [see Fig. 2(d), for example]. The surface morphological images of columnar films, which seem to have a characteristic column–column separation, inspire an investigation of the existence of wavelength selection (periodicity or column–column correlation) and its relation to shadowing effects. Also, similar to the well known scaling behavior $\xi \sim t^{1/z}$ of correlation length ξ (typical feature size in lateral directions) with growth time t and dynamic exponent z[48] during a typical normal incidence deposition, a similar scaling rule like $W \sim d^p$ can also be sought between the average column width W and column length d.[49]

II. EXPERIMENT

Two experimental setups were used for the oblique angle depositions: (1) dc magnetron sputter deposition and (2) thermal evaporation. Experimental details were given in Ref. 46. Both systems included computer controlled sample tilt and rotation (~30 rpm). Tungsten films were deposited by magnetron sputtering, and silicon, cobalt, and copper films were grown by thermal evaporation. The deposition angle was set to $\theta = 87°$ for W and 85° for Si, Co, and Cu depositions.

A. Power law growth of columnar width

In Figs. 2(a)–2(d) we show the cross sections of SEM images of representative Si, Co, Cu, and W films. As we can see from these images, after an initial nucleation of islands, the dominant columns grow as a function of time while some secondary columns stop growing. A salient feature of these columnar structures is that the width, W, of these columns appears to grow in time, or the length of the column, d. To study quantitatively the growth behavior of the columns, we plot in Fig. 2(e) the width, W, as a function of d in log–log scale. A linear relationship for all the columns is found in this plot for all materials studied. The growth is interpreted as a power law growth with the relationship $W \sim d^p$, where the growth exponent $p \sim 0.28–0.34$.[49]

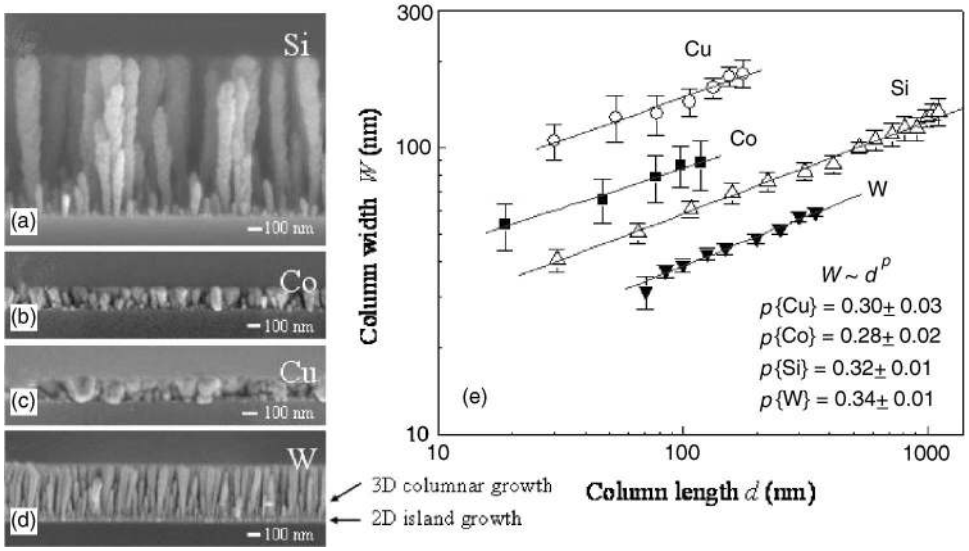

FIG. 2. Cross-sectional scanning electron micrographs of isolated nanocolumnar structures: (a) Si, (b) Co, (c) Cu, and (d) W. The scale bar is 100 nm. (e) The average column width W is plotted as a function of column length d for the materials studied.

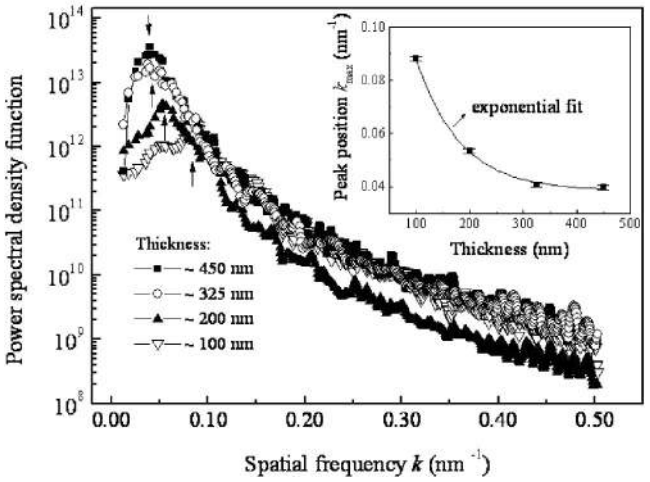

FIG. 3. Power spectral density (PSD) function curves calculated for different thicknesses of tungsten nanocolumns. The peak position corresponds to the spatial frequency of the quasiperiodic structure. The inset shows the change of the maximum peak in spatial frequency as a function of thickness.

B. Quasiperiodic nature of surface morphology growth

The quantitative surface morphology was measured using contact-mode atomic force microscopy (AFM) (Park Scientific Auto CP). The radius of the silicon tip is about 10 nm, and the side angle is about 12°. The scan sizes were 500 $\times$500 nm^2 with 512$\times$512 pixels. We analyzed the quasiperiodic evolution of the nanocolumns by using the method of power spectral density (PSD) analysis. PSD, which is a Fourier transform of surface heights, from a discrete height profile can be estimated as[50]

$$\mathrm{PSD}(k_x,k_y)=\frac{1}{N_xN_y}\left|\sum_{m=1}^{N_x}\sum_{n=1}^{N_y} z(m,n)e^{-imk_x\Delta x-ink_y\Delta y}\right|^2, \tag{1}$$

where N_x and N_y are the dimensions of a discrete surface along the x and y directions, respectively; $k=\sqrt{k_x^2+k_y^2}$ represents the spatial frequency with wavelength λ ($k=2\pi/\lambda$). Furthermore, for an isotropic surface PSD can be circularly averaged in order to obtain better statistics

$$\mathrm{PSD}(k)=\frac{1}{N_k}\sum \mathrm{PSD}(k_x,k_y)|_{k=\sqrt{k_x^2+k_y^2}}, \tag{2}$$

where N_k is the number of points at constant distance k, and the summation is over all points having the same distance.

Figure 3 plots the PSD curves obtained by applying Eq. (2) to the height data of columnar tungsten surfaces measured by AFM. It was observed that the surfaces contain a clear PSD peak of maximum value at a well-defined spatial frequency $k_{\max}$. The shape of the PSD intensity distribution, which is centered at $k_{\max}$, sharpens with the increase of thickness. This reflects the improvement of the quasiperiodic nature of the growth morphology. The shift of the PSD peak versus thickness is shown as the inset of Fig. 3. The fit to the data reveals that the change of the peak position has an exponential decay form ($k_{\max}\sim k_o+be^{-ad}$, where d is the thickness and k_o, a, b are constants). This implies that the spatial wavelength increases with the thickness. On the other hand, the films deposited at normal incidence did not show any clear PSD peak.

III. SIMULATIONS

In order to understand the growth behavior, we used a (2+1) dimensional Monte Carlo method to simulate the growth of the columns produced by the oblique angle deposition.[49] The lattice is formed by cubic lattice points and each incident atom has the dimension of one lattice point. In the study of initial stages of growth, the three-dimensional lattice does not allow overhangs. However, overhangs for the simulations of later stages of columnar growth are included. The simulations include an obliquely incident flux, substrate rotation, and surface diffusion. We assume a uniform flux of atoms approaching the surface at an angle θ. At each simulation step an atom is sent towards a randomly chosen lattice point on the surface of size $L\times L$. To take into account the substrate rotation, each atom is sent with a change in the azimuthal angle of $\Delta\phi$ degrees from the previous one. After the incident atom is deposited onto the surface, an atom is chosen randomly to diffuse to another nearest neighbor random location. The diffusion step is repeated until the assigned number of jumps (D) is made. Then another atom is sent and the deposition and diffusion steps are repeated in a similar way. Our simulations typically involved a system size of $L\times L\times N=512\times512\times512$ with a periodic boundary condition, $\Delta\phi\sim0.04°$, and were conducted for different values of deposition angles and surface diffusion hops.

A. Oblique angle dependent growth (diffusion set to zero)

To see the effects of oblique angle more clearly, we set the surface diffusion rate to zero ($D=0$) for the 2D growth at initial times. Figures 4(a)–4(c) show plots of average island size S (calculated from islands with size $s>1$), island density N (cluster of atoms excluding monomers), and island size distribution N_s (density of islands of size s with $s>1$) at various deposition angles and coverages Θ. The coverage is defined as $\Theta=Ft$ (F is the deposition rate and t is the deposition or simulation time. Θ corresponds to average film thickness in our case). Larger island densities and average island sizes at small coverages suggest that oblique angle promotes the island formation starting from initial times. This can be explained by the enhancement in island formation through the shadowing effect. Shadowing promotes the preferential growth of surface features with greater heights. This gives more chances to monomers at initial times of the growth to capture incident particles and form islands. At larger coverages, we realize that large deposition angles slow down the coalescence process: island density values are higher [Fig. 4(b)] while average island sizes are smaller [Fig. 4(a)] for larger deposition angles. These islands grow preferentially in the vertical direction and manage to survive in the coalescence.

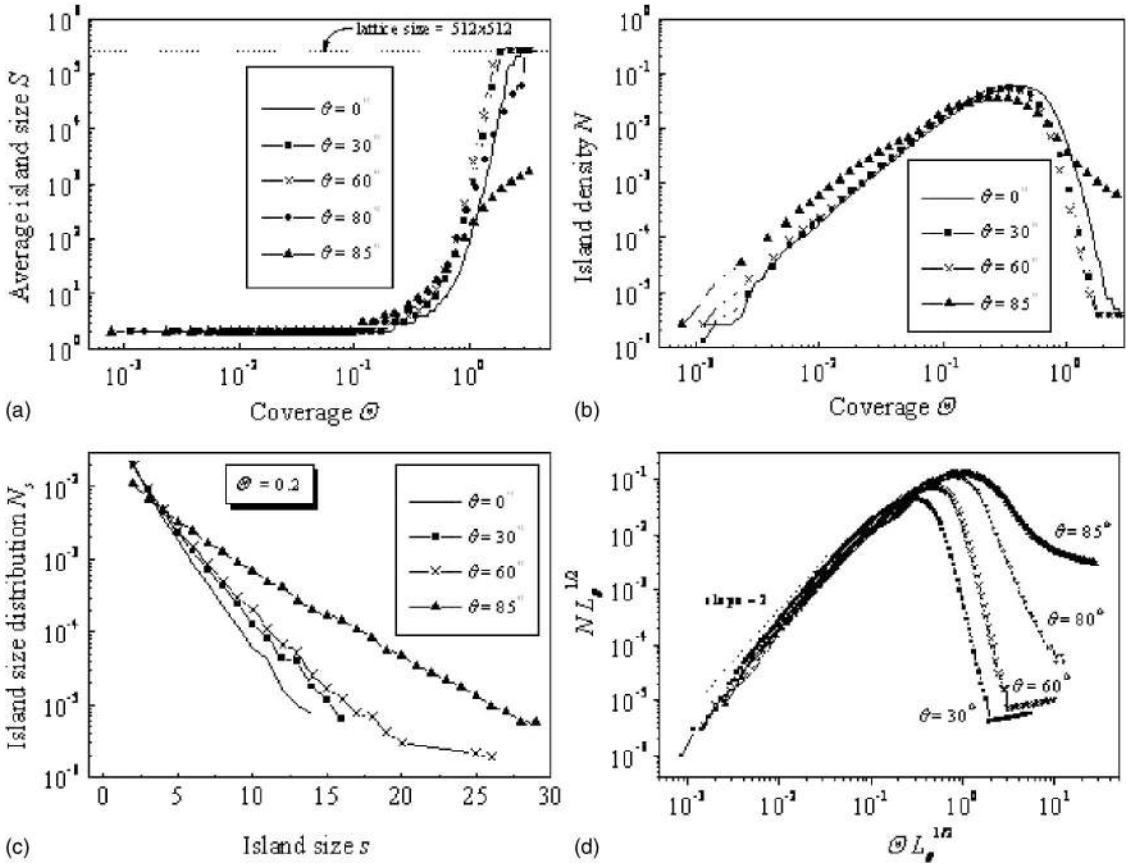

FIG. 4. Average island size (a), island density (b), and island size distribution (c) obtained from simulations at various deposition angles and coverages. (d) Island densities are rescaled using shadowing length.

B. Concept of shadowing length and scaling in island density

In fact, the shadowing effect explained above mimics the effect of surface diffusion. The only difference is that, in the case of shadowing, the incident atom is caught before arriving on the surface. On the other hand, in surface diffusion, an adatom joins the existing monomer or island by hopping through some distance, known as the "diffusion length." Therefore, the lateral distance shadowed by a surface object, which we call "shadowing length," can play the role of diffusion length. We calculated the shadowing length by an island of height h as

$$L_\theta = h \tan(\theta), \tag{3}$$

where $h=1$ for monomers.

Amar, Family, and Lam[45] and Bartelt and Evans[46,47] were able to rescale island densities to become independent of diffusion rates for a normal incidence deposition. Using the analogy between shadowing length and diffusion length, we were able to rescale the island densities as $\hat{N}=NL_\theta^{1/2}$ and $\Theta=\Theta L_\theta^{1/2}$ to become independent of a deposition angle as shown in Fig. 4(d). This supports the idea that shadowing and surface diffusion both have similar effects in the mechanisms of island formation.

C. Phase diagram of quasiperiodic wavelength selection

As shown in Fig. 5(a), stronger PSD peaks start to appear at larger angles. In addition, the phase diagram in Fig. 5(b) illustrates that the quasiperiodic morphology becomes clearer at larger angles and higher film thickness. Due to the preferential growth on taller islands, as the growth transforms from 2D to 3D growth we can expect to see a similar wavelength selection for thicker columnar films. Figure 5(c) plots the PSD peaks for a columnar structure obtained by the simulations that included overhangs and diffusion (see the inset for a cross sectional view of the representative columnar film). The simulations without diffusion also give rise to formation of similar wavelength selection [see the $D=0$ curve in Fig. 5(d)] although this case has smaller PSD peak intensities at similar thicknesses. In addition, the spatial frequency k of periodicity decreases exponentially with the increase of the film thickness [Fig. 5(d)] or decreases linearly with the increase of the deposition angle through shadowing length $L_\theta \sim \tan\theta$ [Fig. 5(a) inset]. Since shadowed columns see no flux of incoming material and cease to grow, the number density of columns decreases with height that results in larger separations and therefore smaller spatial frequencies. Our simulations agree well with the experimental results shown in Fig. 3.

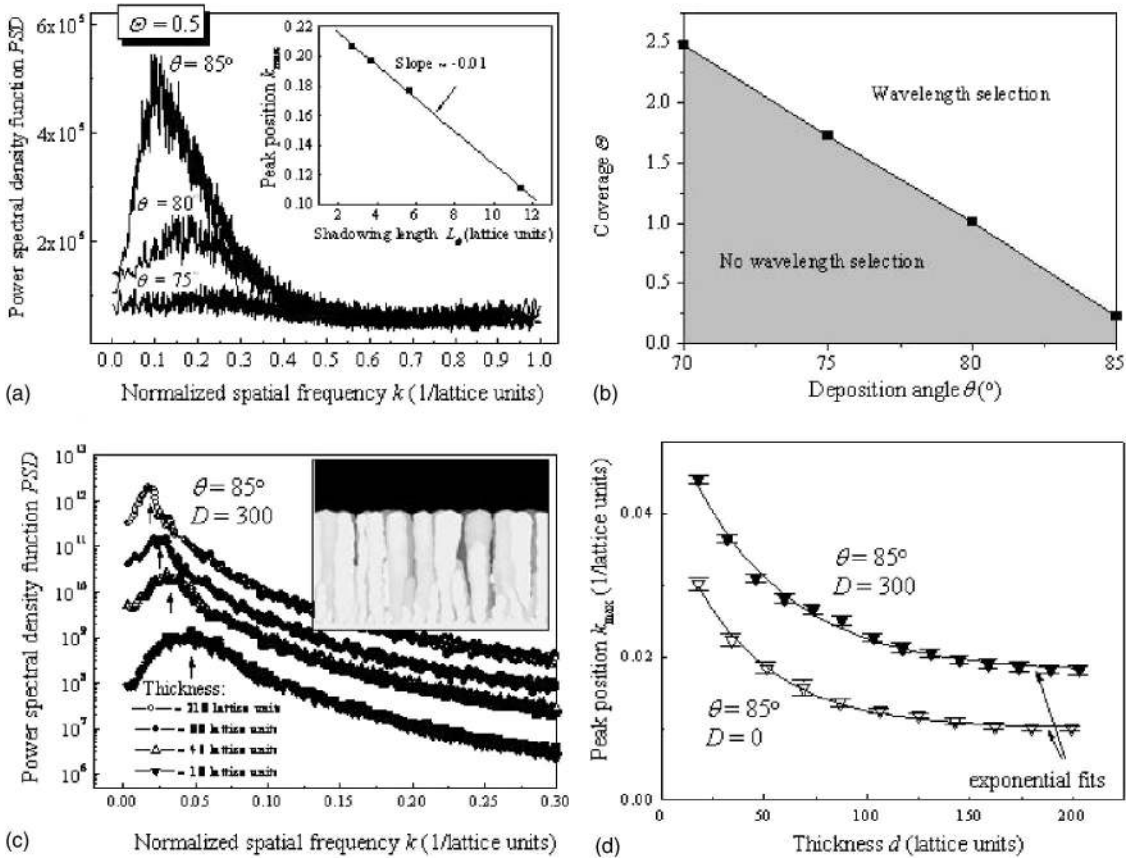

FIG. 5. (a) Power spectral density function profiles obtained from simulations are plotted for different deposition angles at the initial stages of 2D island growth. The inset plots the peak position as a function of shadowing length, where we used $L_\theta \sim \tan(\theta)$. (b) A diagram showing the wavelength selection as functions of coverage and deposition angle. (c) PSD function curves at later stages of 3D columnar growth. (d) The maximum PSD peak positions in spatial frequency as a function of thickness for 85° incident angle and $D=0$ (inverse open triangles) and $D=300$ (inverse filled triangles).

D. Diffusion dependent scaling exponent for column width

In addition, in order to analyze the evolution of column width W, simulations (with overhangs) were conducted for different values of D ranging from 0 to 4×10^3. After each simulation, W as a function of column length d is calculated by slicing the film layer by layer parallel to the substrate plane. The log–log plot in Fig. 6(a) reveals that the simulated column widths also have a power law dependence on d. The exponent p at a given D is shown in Fig. 6(b). When the diffusion rate approaches zero, p is found to approach 0.5. With increasing diffusion rates, the value of p "crosses over" from 0.5 to 0.3. Our experimental values of p are in between 0.5 and 0.3, but closer to 0.3. We therefore believe that our simulation results are consistent with our experimental measurements.

IV. ANALYTICAL MODELS

Meakin and Krug reported earlier their theoretical study on the oblique angle deposition (θ approaches 90°) without substrate rotation.[33,51] Surface diffusion was not included in their study. They investigated the evolution of column edges when the columns were cross sectioned through a plane parallel to a substrate. They found that "cluster edges evolve according to a growth process reminiscent of the two-dimensional Eden model, and hence their fluctuations can be described by the well-known Kardar–Parisi–Zhang (KPZ) equation for a one-dimensional moving interface." They identified the surface correlation lengths ξ_x and ξ_y to be the column widths in the x and y directions parallel to the substrate, respectively. The incident beam on the substrate is in the x direction and is perpendicular to the y direction. These column widths were shown to correspond to the correlation lengths of the (1+1)-dimensional KPZ interface,[52] with $\xi_x \sim d^{p_x}$, and $\xi_y \sim d^{p_y}$, where

$$p_x(\mathrm{KPZ}) = \tfrac{1}{3} \quad \text{and} \quad p_y(\mathrm{KPZ}) = \tfrac{2}{3}.$$

These results are applicable when the substrate stays stationary during a deposition. In our case of substrate rotation one would expect $W \sim \sqrt{\xi_x \xi_y} \sim \sqrt{d^{p_x+p_y}} = d^{(p_x+p_y)/2} \equiv d^p$, with the scaling exponent $p(\mathrm{KPZ}) = (p_x+p_y)/2 = (1/3+2/3)/2 = 1/2 = 0.50$. (The cross section area of the column is the product of ξ_x and ξ_y.) Therefore, only one growth exponent is required to describe the growth and the structure is symmetric in the x and y directions.

By using a similar argument we can incorporate the effect of diffusion by starting with the (1+1)-dimensional model of

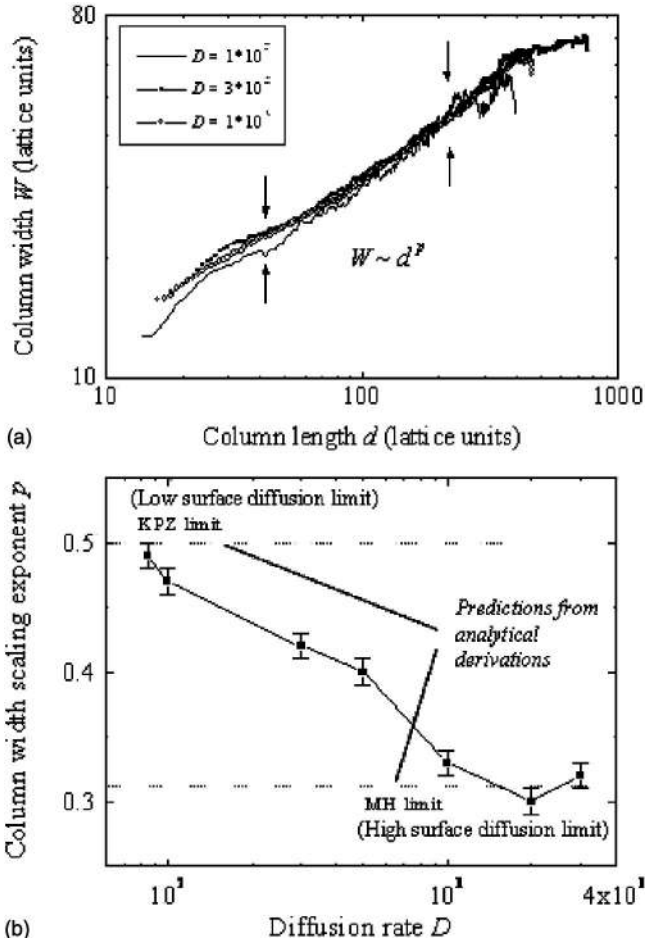

FIG. 6. (a) Simulated average column widths as a function of column length are plotted for various diffusion rates. The vertical arrows indicate the region used for determining the scaling exponent p. (b) Scaling exponent p calculated for various diffusion rates are shown. The dotted lines represent the predictions from KPZ limit and MH limit obtained by analytic solutions.

Mullins–Herring (MH) (see p. 142 in Ref. 45). In the MH model, surface diffusion and noise are the mechanisms that control the growth and would give

$$p_x(\mathrm{MH}) = \tfrac{3}{8} \quad \text{and} \quad p_y(\mathrm{MH}) = \tfrac{1}{4}$$

when the substrate stays stationary during a deposition. For the present case of substrate rotation, we thus have

$$p(\mathrm{MH}) = \frac{(p_x + p_y)}{2} = \frac{3/8 + 1/4}{2} = \frac{5}{16} \sim 0.31.$$

Therefore, in the (2+1)-dimensional oblique angle deposition with substrate rotation, we expect the column width scaling exponent should cross over from $p(\mathrm{KPZ}) = 0.50$ for pure shadowing with no diffusion to $p(\mathrm{MH}) = 0.31$ for both shadowing and surface diffusion.[49] In addition, our simulation results agree well with these estimations [see Fig. 6(b), dotted lines]. There exists a competition between shadowing and diffusion. Shadowing tends to make columns grow wider while diffusion forces columns to grow towards the columnar axes.

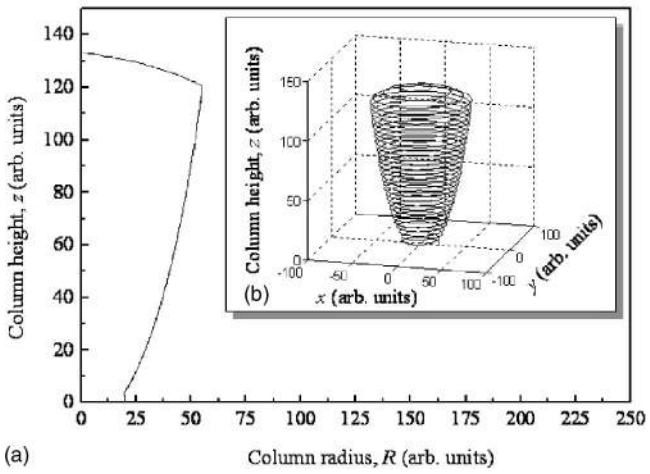

FIG. 7. (a) Radius R of the column is simulated as a continuous, single-valued function of height z. (b) The (2+1)-dimensional interpretation of (a).

In addition to the approach above, we derived a continuum equation to describe the growth of an isolated column's radius as a function of its height coordinate and time

$$\frac{\partial R}{\partial t} = F \cdot g \cdot \sqrt{1 + (\nabla R)^2} + \eta(z,t), \tag{4}$$

where F is the flux of a material at angle θ, R is the column radius (as a function of height, z, and time, t), and $\eta(z,t)$ is the noise term. The term g is a shadowing function, equal to 0 at positions along the column that are shadowed from the flux of incoming particles, and 1 elsewhere. The differential term in Eq. (4) allows the growth in a direction parallel to surface normal. The column may start growing from an initial seed element of height z_0. Note that we set the z axis as the column height, which is an *independent* variable, and the x axis as the column radius, a *dependent* variable. Figures 7(a) and 7(b) show the 2D and 3D interpretations of an isolated column, respectively, obtained by a numerically calculation using Eq. (4) (with a spherical seed radius=20 units, seed–seed separation $l = 200$ units, and $\theta = 85°$).

For a rotationally symmetric column growing from a flat surface, substituting $R = W/2$ and $z - z_0 = d$ (the height of initial seed $z_0 = 0$ for our case and therefore $z = d$) into $W \sim d^p$ we obtain $R \sim z^p$. Therefore we can extract exponent p from the numerically obtained columns through Eq. (4). Therefore, we calculated p values for various given column–column separations l in the range 100–275 units. The term p did not change significantly with l, and after averaging, we obtained the approximate growth exponent value $p \sim 0.37 \pm 0.02$. This is slightly greater than the experimental values $p \sim 0.28$–0.34 obtained for various nanocolumns. However, if we were to include surface diffusion in Eq. (4), we would expect smaller p values. In addition, inclusion of the effects of an angular spread in incident flux, or an incident atom sticking probability not equal to 1 may further reduce the exponent values.

V. CONCLUSION

In conclusion, we have presented a detailed theoretical and experimental study of the growth dynamics during oblique angle deposition. The growth regimes investigated covered the deposition times from very early stages of island growth to later stages of 3D nanocolumns. It has been shown that shadowing effect introduces preferential growth on taller surface heights and therefore enhances the island formation even in the absence of surface diffusion. The concept of shadowing length has been defined quantitatively and was shown to mimic the effects of surface diffusion length. By this method, it has been shown that a scaling form exists for the island densities, independent of the deposition angle except at high coverages. In addition, the wavelength selection that gives rise to quasiperiodic morphologies has been shown to exist during oblique angle growth, which was not observed for continuous films deposited at normal incidence. We also have shown that there is a scaling relationship for the evolution of isolated columnar width of various materials with column length. We showed that column width changes with column length according to a power law with the exponent $p \sim 0.28-0.34$. It was argued that the growth exponent should cross over from 0.50 with pure shadowing and no surface diffusion to 0.31 with both shadowing and surface diffusion. The exponent values calculated from a derived continuum equation were consistent with the experimental results and gave further insight to the understanding of growth dynamics. The unique geometrical shapes from a large variety of materials produced by oblique angle deposition suggest that shadowing effects can be used as an efficient tool to understand and control the growth morphologies formed by many other traditional deposition techniques.

ACKNOWLEDGMENTS

This work was supported in part by the NSF. T. K. was supported by the Harry F. Meiners Fellowship.

[1]N. O. Young and J. Kowal, Nature (London) **183**, 104 (1959).
[2]T. Motohiro and Y. Taga, Appl. Opt. **28**, 2466 (1989).
[3]R. M. Azzam, Appl. Phys. Lett. **61**, 3118 (1992).
[4]K. Robbie, L. J. Friedrich, S. K. Dew, T. Smy, and M. J. Brett, J. Vac. Sci. Technol. A **13**, 1032 (1995).
[5]K. Robbie, M. J. Brett, and A. Lakhtakia, Nature (London) **384**, 616 (1996).
[6]Y.-P. Zhao, D.-X. Ye, G.-C. Wang, and T.-M. Lu, Nano Lett. **2**, 351 (2001).
[7]K. Robbie and M. J. Brett, J. Vac. Sci. Technol. A **15**, 1460 (1997).
[8]P. I. Rovira, R. A. Yarussi, R. W. Collins, V. C. Venugopol, A. Lakhtakia, R. Messier, K. Robbie, and M. J. Brett, Thin Solid Films **313**, 373 (1998).
[9]I. Hodgkinson, Q. H. Wu, and J. Hazel, Appl. Opt. **37**, 2653 (1998).
[10]I. Hodgkinson, B. Knight, A. Lakhtakia, and K. Robbie, Appl. Opt. **39**, 642 (2000).
[11]I. Hodgkinson, Q. H. Wu, and S. Collett, Appl. Opt. **40**, 452 (2001).
[12]M. W. Seto, K. Robbie, D. Vick, M. J. Brett, and L. Kuhn, J. Vac. Sci. Technol. B **17**, 2172 (1999).
[13]M. W. Seto, B. Dick, and M. J. Brett, J. Micromech. Microeng. **11**, 582 (2001).
[14]D.-L. Liu, D.-X. Ye, F. Khan, F. Tang, B.-K. Lim, R. C. Picu, G.-C. Wang, and T.-M. Lu, J. Nanosci. Nanotechnol. **3**, 492 (2003).
[15]F. Liu, M. T. Umlor, L. Shen, J. Weston, W. Eads, J. A. Barnard, and G. J. Mankey, J. Appl. Phys. **85**, 5486 (1999).
[16]B. Dick, M. J. Brett, T. J. Smy, M. R. Freeman, M. Malac, and R. F. Egerton, J. Vac. Sci. Technol. A **18**, 1838 (2000).
[17]F. Tang, D.-L. Liu, D.-X. Ye, Y.-P. Zhao, T.-M. Lu, G.-C. Wang, and A. Vijayaraghavan, J. Appl. Phys. **93**, 4194 (2003).
[18]M. Malac and R. F. Egerton, J. Vac. Sci. Technol. A **19**, 158 (2001).
[19]B. Djurfors, M. J. Brett, and D. G. Ivey, Mater. Res. Soc. Symp. Proc. **749**, W5.4.1 (2003).
[20]J. P. Singh, G.-R. Yang, T.-M. Lu, and G.-C. Wang, Appl. Phys. Lett. **81**, 4601 (2002).
[21]O. Toader and S. John, Science **292**, 1133 (2001).
[22]O. Toader and S. John, Phys. Rev. E **66**, 016610 (2002).
[23]M. J. Colgan and M. J. Brett, Thin Solid Films **389**, 1 (2001).
[24]M. J. Colgan, D. Vick, and M. J. Brett, Mater. Res. Soc. Symp. Proc. **636**, D9.24.1 (2001).
[25]T. Smy, D. Walkey, K. D. Harris, and M. J. Brett, Thin Solid Films **391**, 88 (2001).
[26]K. D. Harris, D. Vick, E. J. Gonzales, T. Smy, K. Robbie, and M. J. Brett, Surf. Coat. Technol. **138**, 185 (2001).
[27]K. D. Harris, M. J. Brett, T. Smy, and C. Backhouse, J. Electrochem. Soc. **147**, 2002 (2000).
[28]M. Seto, K. Westra, and M. J. Brett, J. Mater. Chem. **12**, 2348 (2002).
[29]Y.-P. Zhao, D.-X. Ye, P.-I. Wang, G.-C. Wang, and T.-M. Lu, Int. J. Nanosci. **1**, 87 (2002).
[30]M. Malac, R. F. Egerton, M. J. Brett, and B. Dick, J. Vac. Sci. Technol. B **17**, 2671 (1999).
[31]B. Dick, M. J. Brett, T. Smy, M. Belov, and M. R. Freeman, J. Vac. Sci. Technol. B **19**, 1813 (2001).
[32]K. Robbie, J. C. Sit, and M. J. Brett, J. Vac. Sci. Technol. B **16**, 1115 (1998).
[33]P. Meakin and J. Krug, Phys. Rev. A **46**, 3390 (1992).
[34]R. Messier, V. C. Venugopal, and P. D. Sunal, J. Vac. Sci. Technol. A **18**, 1538 (2000).
[35]P. Meakin and J. Krug, Phys. Rev. A **46**, 4654 (1992).
[36]T. Nagatani, J. Phys. A **24**, L449 (1991).
[37]J. M. Nieuwenhuizen and H. B. Haanstra, Philips Tech. Rev. **27**, 87 (1966).
[38]R. N. Tait, T. Smy, and M. J. Brett, Thin Solid Films **226**, 196 (1993).
[39]K. D. Harris, D. Vick, T. Smy, and M. J. Brett, J. Vac. Sci. Technol. A **20**, 2062 (2002).
[40]Paritosh and D. J. Srolovitz, J. Appl. Phys. **91**, 1963 (2002).
[41]D.-X. Ye, Y.-P. Zhao, G.-R. Yang, Y.-G. Zhao, G.-C. Wang, and T.-M. Lu, Nanotechnology **13**, 615 (2002).
[42]D. Vick, T. Smy, and M. J. Brett, J. Mater. Res. **17**, 2904 (2002).
[43]T. Smy, D. Vick, M. J. Brett, S. K. Dew, A. T. Wu, J. C. Sit, and K. D. Harris, J. Vac. Sci. Technol. A **18**, 2507 (2000).
[44]M. Suzuki and Y. Taga, J. Appl. Phys. **90**, 5599 (2001).
[45]J. G. Amar, F. Family, and P.-M. Lam, Phys. Rev. B **50**, 8781 (1994).
[46]M. C. Bartelt and J. W. Evans, Phys. Rev. B **46**, 12675 (1992).
[47]J. W. Evans and N. C. Bartelt, J. Vac. Sci. Technol. A **12**, 1800 (1994).
[48]A.-L. Barabasi and H. E. Stanley, *Fractal Concepts in Surface Growth* (Cambridge University Press, Cambridge, England, 1995).
[49]T. Karabacak, J. P. Singh, Y.-P. Zhao, G.-C. Wang, and T.-M. Lu, Phys. Rev. B **68**, 125408 (2003).
[50]Y.-P. Zhao, G.-C. Wang, and T.-M. Lu, *Characterization of Amorphous and Crystalline Rough Surface: Principles and Applications* (Academic, San Diego, 2001), p. 28.
[51]P. Meakin and J. Krug, Europhys. Lett. **11**, 7 (1990).
[52]M. Kardar, G. Parisi, and Y.-C. Zhang, Phys. Rev. Lett. **56**, 889 (1986).